New insights into the gas-phase unimolecular fragmentations of [Cysteine–Ca]2+ complexes

ARTICLE *in* COMPUTATIONAL AND THEORETICAL CHEMISTRY · NOVEMBER 2014

Impact Factor: 1.55 · DOI: 10.1016/j.comptc.2014.08.015

5 AUTHORS, INCLUDING:

Marcela Hurtado

Universidad Autónoma de Madrid

20 PUBLICATIONS **84** CITATIONS

SEE PROFILE

Otilia Mó

Universidad Autónoma de Madrid

403 PUBLICATIONS **6,379** CITATIONS

SEE PROFILE

Manuel Yanez

Universidad Autónoma de Madrid

271 PUBLICATIONS **3,747** CITATIONS

SEE PROFILE

Al Mokhtar Lamsabhi

Universidad Autónoma de Madrid

70 PUBLICATIONS **805** CITATIONS

SEE PROFILE

Computational and Theoretical Chemistry 1047 (2014) 38–46

Contents lists available at ScienceDirect

Computational and Theoretical Chemistry

journal homepage: www.elsevier.com/locate/comptc

New insights into the gas-phase unimolecular fragmentations of [Cysteine–Ca]$^{2+}$ complexes

Marcela Hurtado [a,*], Otilia Mó [a], Manuel Yáñez [a], Barbara Herrera [b], Al Mokhtar Lamsabhi [a,*]

[a] Departamento de Química, Módulo 13, Universidad Autónoma de Madrid, Campus de Excelencia UAM-CSIC Cantoblanco, 28049 Madrid, Spain
[b] Laboratorio de Química Teórica Computacional (QTC), Facultad de Química, Pontificia Universidad Católica de Chile, Santiago, Chile

ARTICLE INFO

Article history:
Received 29 May 2014
Received in revised form 12 August 2014
Accepted 13 August 2014
Available online 25 August 2014

Keywords:
Cysteine
Gas-phase reactions
Ca^{2+}
Coulomb explosion
Neutral loss
Reaction electronic flux

ABSTRACT

The dominant fragmentation processes in the gas phase of the doubly-charged complexes formed by the association of Ca^{2+} to cysteine, namely the loss of ammonia and the formation of ammonium ion, have been analyzed in detail in terms of the reaction force profiles, the chemical potential and the reaction electronic flux (REF) calculated at the B3LYP/6-311+G(d,p) level of theory. These analyses show that the investigated ammonia-loss processes can be classified as elementary reactions, whereas the Coulomb explosions yielding $NH_4^+ + [CaC_3H_3O_2S]^+$ include, at least two elementary steps. The variations of the chemical potential and in particular of the REF permits to identify very easily the subtle differences that exist between processes, such as the ammonia-loss ones which are apparently equal. The bond breaking and the bond formation processes can be followed through the evolution of the corresponding internuclear distances along the reaction coordinate; but the most precise information on where the bond formation or the bond fissions are complete is readily obtained by examining the derivatives of the corresponding bond orders along the reaction coordinate.

1. Introduction

The study of the unimolecular reactivity of a complex based on its mass spectrum is not a simple task. The different pathways or mechanisms that are proposed to explain the experimental findings are in many cases difficult to establish in an unambiguous way because of the high number of possibilities that should be traced and analyzed in detail.

In this respect, high-level theoretical calculations are of a great importance to propose the most likely mechanism both on thermodynamic and kinetic grounds [1]. Usually, a reasonable agreement between theory and experiment based on the relative thermodynamic stabilities of the different stationary points on the potential energy surface (PES) is considered sufficient to explain the main features of the observed mass spectra, in particular when dealing with doubly-charged species where Coulomb explosions and neutral-loss processes compete [2–23]. However, in some cases the same precursor can be involved in different competing mechanisms, and a closer look to the factors favoring one evolution versus the other is unavoidable if a complete picture of both mechanisms is envisaged. This is the case of the gas-phase reactions between cysteine (Cys) and Ca^{2+} in which the fragmentation [23] of $[Ca(Cys)]^{2+}$ ions are dominated by three competitive processes: the loss of ammonia yielding a lighter doubly charged ion $[CaC_3H_4O_2S]^{2+}$, a Coulomb explosion yielding $NH_4^+ + [CaC_3H_3O_2S]^+$, and the loss of H_2S. Although the general mechanisms behind these processes have been proposed using DFT calculated potential energy surfaces [23], some details still require further analysis. In fact, both, the loss of ammonia and the Coulomb explosion have the same precursors: salt-bridge dications in which a NH_3 is attached to the C in the α-position with respect to the CO_2 group [23]. It seems then necessary to have a new perspective on the two kind of processes to really know how the system evolves through one way or the other. A good way to gain some insight into the peculiarities of both competitive mechanisms is through the reaction force theory because it permits to analyze the evolution of the system through the variations of the chemical potential and the electronic flux along the corresponding reaction coordinate. This specific analysis is the aim of this paper.

2. Theoretical framework

2.1. Energy and reaction force

A chemical reaction can be understood in terms of geometrical changes of the molecular structures and reordering of the electron

* Corresponding authors.

http://dx.doi.org/10.1016/j.comptc.2014.08.015
2210-271X/

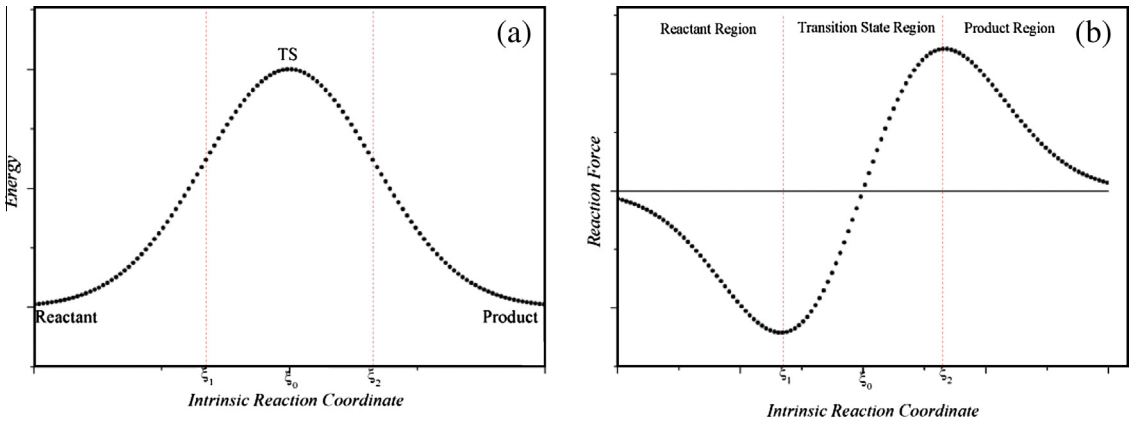

Fig. 1. Energy (a) and force (b) profiles for an elementary reaction connecting reactants (**R**) and products (**P**).

densities involved in the process and can be analyzed in terms of the reaction force concept [24–26] which permits to define regions where specific atomic or molecular interactions are taking place during the reaction [27,28].

In any chemical reaction the reactant is transformed into product through a series of continuum structural and electronic changes, which are represented via a minimum energy profile ($E(\xi)$) that links the transition state to the reactants and products [24] (see Fig. 1a). Along the intrinsic reaction coordinate (IRC = ξ), the reaction force is defined as the negative of the derivative of the energy, $E(\xi)$, with respect to reaction coordinate ξ by the expression,

$$F(\xi) = -\frac{dE(\xi)}{d\xi} \tag{1}$$

For any elementary step, the reaction force is characterized by a minimum and a maximum located at ξ_1 and ξ_2, respectively (see Fig. 1b) which delimitate three regions along the reaction coordinate.

A first one ($\xi_R \leqslant \xi \leqslant \xi_1$) in which the reactants are prepared for the reaction mainly through structural reordering. A second one ($\xi_1 \leqslant \xi \leqslant \xi_2$) which corresponds to the region where most electronic changes due to bond formation and breaking take place, and that can be associated with the transition state. Finally, a third region, ($\xi_2 \leqslant \xi \leqslant \xi_P$), in which the structural relaxation to reach the products of the reaction takes place. The definition of these three regions permits an easy evaluation of the activation energy $\Delta E^{\neq}$ and the reaction energy ΔE^0 in terms of reactions works [29],

$$\Delta E^{\neq} = W_1 + W_2 \tag{2}$$

where,

$$W_1 = -\int_{\xi_R}^{\xi_1} F(\xi)d\xi > 0 \quad \text{and} \quad W_2 = -\int_{\xi_1}^{\xi_0} F(\xi)d\xi > 0 \tag{3}$$

Similarly the reaction energy can be defined as:

$$\Delta E_R = W_1 + W_2 + W_3 + W_4 \tag{4}$$

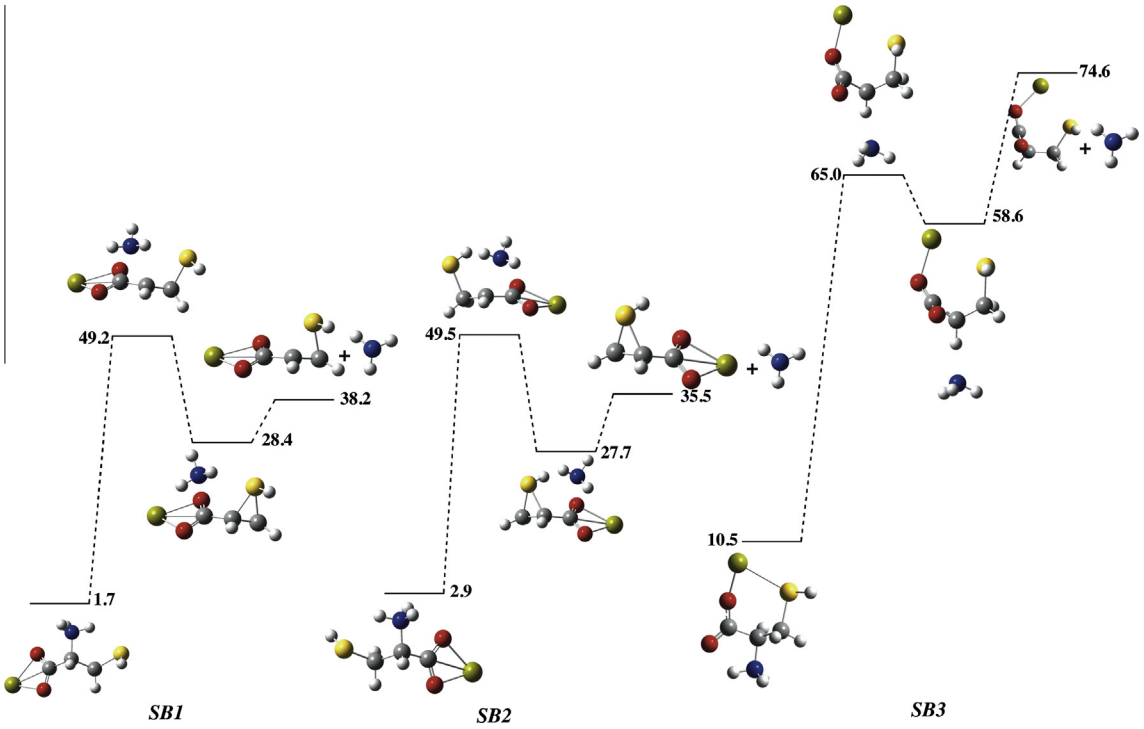

Fig. 2. Enthalpy profiles associated with the loss of ammonia from complexes ***SB1***, ***SB2***, and ***SB3***. B3LYP/6-311++G(3df,2p)//B3LYP/6-311+G** relative enthalpies (kcal mol^{-1}) are calculated with respect to the global minimum of the PES, at 298.2 K. Values taken from Ref. [25].

where,

$$W_3 = -\int_{\xi_0}^{\xi_2} F(\xi)d\xi < 0 \quad \text{and} \quad W_4 = -\int_{\xi_2}^{\xi_P} F(\xi)d\xi < 0 \tag{5}$$

Further useful information of the reaction mechanism can be obtained by analyzing the evolution of the chemical potential along the reaction coordinate. The electronic chemical potential, μ, for a system of N electrons, measures the escaping tendency of electrons from high chemical potential sites to low chemical potential ones. It is defined as the derivative of the total energy with respect to N when the external potential, $v(r)$, remains constant and can be reasonably approximated in terms of the ionization energy (IE) and the electron affinity (EA) of the system, or applying Koopman's theorem, in terms of the energies to the highest occupied and lowest unoccupied molecular orbitals, ε_H and ε_L, respectively.

$$\mu = \left(\frac{\partial E}{\partial N}\right)_{v(\vec{r})} \approx -\frac{1}{2}(IE + EA) \approx \frac{1}{2}(\varepsilon_L + \varepsilon_H) \tag{6}$$

Once the chemical potential is known it is possible to evaluate the reaction electronic flux, $J(\xi)$, (REF) as [30,31]:

$$J(\xi) = -\frac{d\mu}{d\xi} \tag{7}$$

so that positive values of $J(\xi)$ should be associated to spontaneous rearrangements of the electron density driven by bond strengthening or bond formation processes, whereas negative values of $J(\xi)$ are associated with non-spontaneous rearrangements of the electron density that are mainly driven by bond weakening or bond breaking processes [32].

2.2. Geometry optimization

All the geometries employed in this study were taken from Ref. [23] and they correspond to B3LYP [33,34] fully optimized geometries using a 6-311++G(d,p) basis set. The intrinsic reaction coordinate (IRC) procedure in which the reaction coordinate, ξ, is expressed in terms of mass-weighted internal coordinates [35] was used to obtain the energy and force profiles of the different reactions under investigation. Harmonic frequency calculations have been carried out for all the stationary points on the PES in order to verify that they correspond to either local minima or transition states. All calculations were performed with the Gaussian09 series of programs [36]. In order to study the bonding changes occurring along the reactions we have calculated the bond orders within the framework of Natural Bond Orbital analysis [37]. The electron density of the systems has been analyzed by means of Atoms In Molecules (AIM) methodology [38,39].

3. Results and discussion

As it was mentioned in the introduction the MS/MS spectrum of $[Cysteine–Ca]^{2+}$ is dominated by three processes where the loss of ammonia or the ammonium ion are the main peaks, being the one corresponding to the deamination of the $[Ca(Cys)]^{2+}$ the most intense one. A detailed exploration of the $[Ca(Cys)]^{2+}$ PES suggested that the loss of ammonia originates in the salt-bridge complexes ***SB1***–***SB3***, which through activation barriers around 200 kJ mol^{-1}, lead to $[C_3O_2H_4SCa]^{2+}$ products that only differ in the local conformation of the HC–CH_2–SH group (see Fig. 2).

It seems however obvious, that the precursors for the Coulomb explosion $NH_4^+ + [CaC_3H_3O_2S]^+$ have to be also salt-bridge complexes (***SB1***–***SB4***), because the formation of an ammonium ion requires precursors in which a NH_3 group is already formed. Two different proton transfers had been envisaged involving either the proton of the thiol group (see Fig. 3a), or the proton from the neighboring –CH_2 group (see Fig. 3b) [23]. In both cases, although the precursors are different, ***SB1*** and ***SB4***, respectively, the mechanisms imply a cleavage of the C–NH_3 bond and the approaching of the ammonia molecule to the proton donor center. However, the different profile of both potential energy curves clearly indicate that the real mechanisms should present some differences, which will be more evident when analyzing the behavior of the forces, the chemical potential and the reaction electronic flux along the corresponding reaction coordinates.

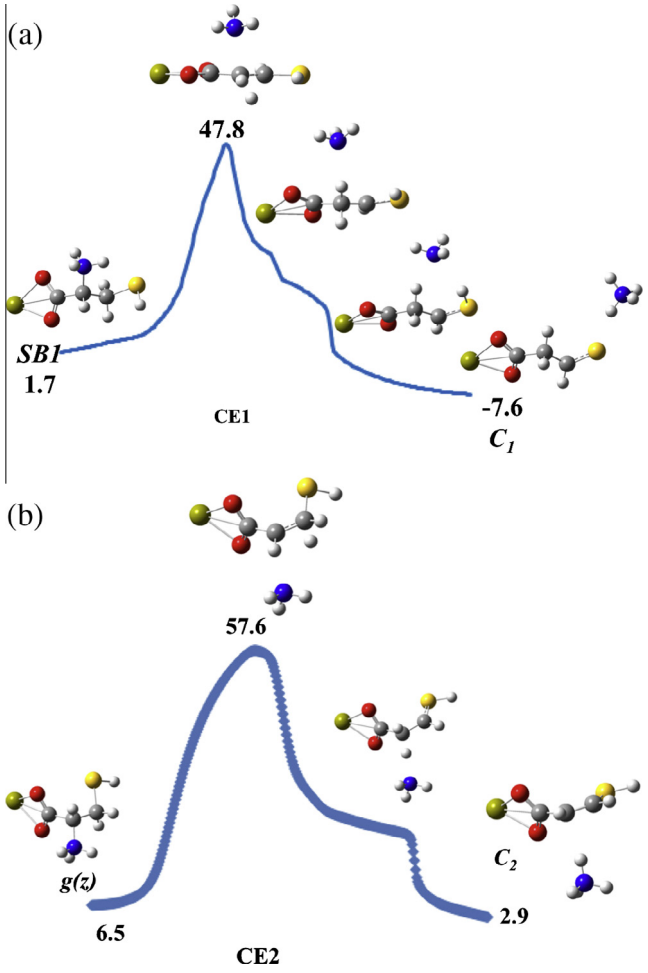

Fig. 3. Potential enthalpy curves corresponding to the two mechanisms associated with the Coulomb explosions yielding NH_4^+. Relative enthalpies (kcal mol^{-1}) are defined with respect to the global minimum of the PES. Values taken from Ref. [25].

3.1. Energy and reaction force profiles

In what follows we will designate as **AL1** and **AL2** the ammonia-loss process with origin in ***SB1*** and ***SB3*** structures, respectively. **CE1** and **CE2** will designate the Coulomb explosions leading to the loss of ammonium ion and with origin in ***SB1*** and ***SB4*** structures, respectively. The energy and force profiles for these four reactions are given in Fig. 4. The different works along the reaction coordinate, as well as the activation barrier ($\Delta E^{\neq}$) and the overall reaction energy have been summarized in Table 1. It can be observed that whereas the two ammonia-loss processes considered in our survey are endothermic, the Coulomb explosions leading to $NH_4^+ + [CaC_3H_3O_2S]^+$ are exothermic, although the corresponding activation barriers for the four processes are not significantly different, the lower one being that associated with the

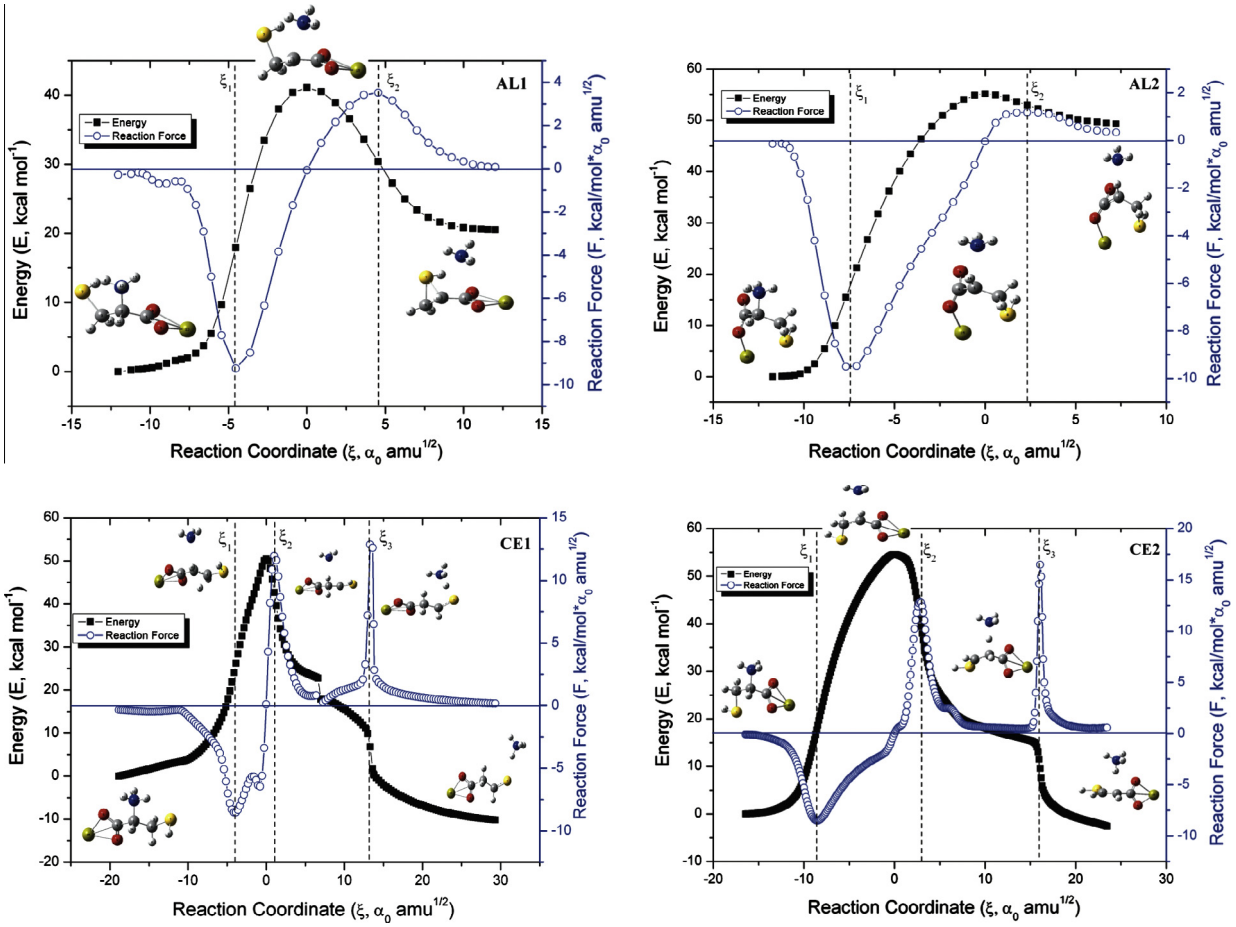

Fig. 4. Energy and force profiles for the **AL1**, **AL2**, **CE1** and **CE2** processes.

Table 1
Energetic data for reactions **AL1**–**CE2**: reaction energy (ΔE^0), activation energy ($\Delta E^{\neq}$) and works performed on and by the systems along the reaction coordinate (*W1*–*W4*) (values are in kcal mol^{-1}).

	ΔE^0	$\Delta E^{\neq}$	*W1*	*W2*	*W3*	*W4*
AL1	20.21	40.46	17.70	22.76	10.34	9.87
AL2	49.17	54.92	15.38	39.54	2.08	3.67
CE1	−9.6	50.25	24.06	26.19	7.60	52.25
CE2	−2.56	54.54	18.68	35.86	13.58	43.52

AL1 process. Also interestingly, in all the cases, the highest percentage of the activation energy ($\Delta E^{\neq}$) corresponds to the reordering of the electronic cloud of reactants (W2) which amounts to 56.25% and 72.00% for **AL1** and **AL2**, respectively and slightly lower values 52.12% and 65.75% for the Coulomb explosions **CE1** and **CE2**, respectively.

The largest difference between the ammonia-loss processes and the Coulomb explosions occurs at the products region. Whereas for ammonia-loss both *W3* and *W4* components are rather similar, for the Coulomb explosions *W4* is from 3 to 7 times larger than *W3*, explaining why these two processes are exothermic. Indeed, the large value of *W4* reflects the energy release associated with the formation of the new N–H bond of the ammonium ion, when the proton transfer process is completed.

However, the most significant differences between both kinds of processes are evident when looking at the reaction force profiles. Whereas the ammonia-loss processes exhibit the typical shape one may expect for an elementary process, with a minimum and a maximum at ξ_1 and ξ_2, respectively, the profile for the Coulomb explosions is more complex, presenting one additional maximum ξ_3 and therefore one additional local minimum between ξ_2 and ξ_3. From Fig. 4 it can be clearly seen that this additional maximum is related with the shoulder observed in the energy profile at ξ_3. The same figure illustrates also the detailed mechanism, showing that the Coulomb explosions can be envisaged as a two-steps process. The first one would correspond to the C–NH_3 bond cleavage with a force profile similar to the ammonia-loss reaction, but when the system is approaching the products region, there is a sudden and further energy decrease associated with the proton transfer toward the NH_3 fragment, which corresponds to the second maximum in the force profile. There are also some subtle differences between the two ammonia-loss and the two Coulomb explosions considered. For the **AL2** reaction the barrier is closer to products than for the **AL1** process. As far as the Coulomb explosions are concerned, it can be noted the existence of a second small shoulder in the energy profile of the **CE1** process which is not observed in the **CE2** reaction.

3.2. Chemical potential and reaction electronic flux

These features are ratified when looking at the behavior of the electronic chemical potential (μ) and the REF along the intrinsic reaction coordinate (see Fig. 5).

At a first glance it is apparent that for both ammonia-loss processes the chemical potential evolves in a rather similar way, the most important changes taking place at the TS region, while it remains almost constant within reactants and products regions.

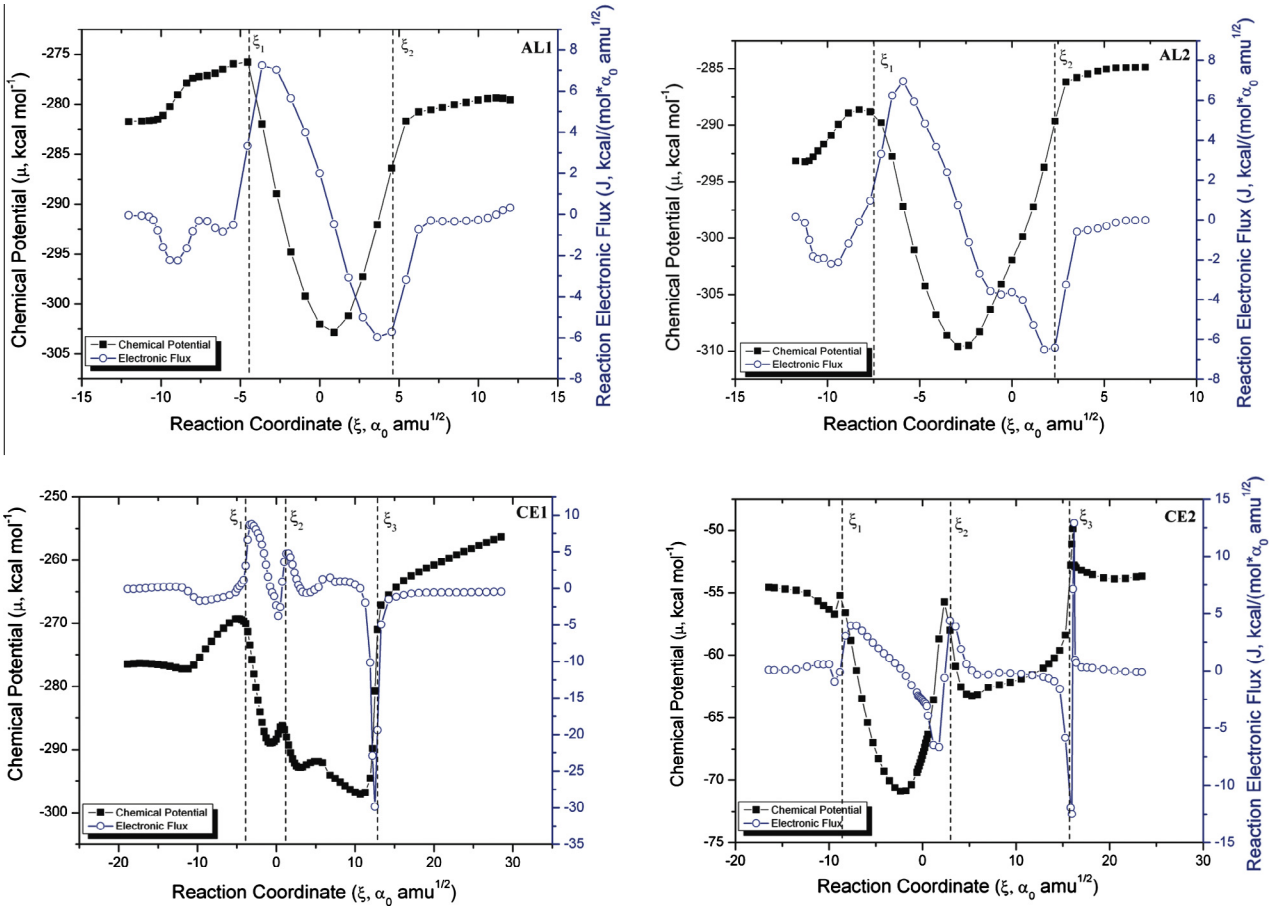

Fig. 5. Evolution of the chemical potential (μ, kcal mol^{-1}, black line) and reaction electronic flux (REF, kcal mol^{-1} α_0 amu^{½}; blue line) along the reaction coordinate for the **AL1**, **AL2**, **CE1** and **CE2** processes. (For interpretation of the references to colour in this figure legend, the reader is referred to the web version of this article.)

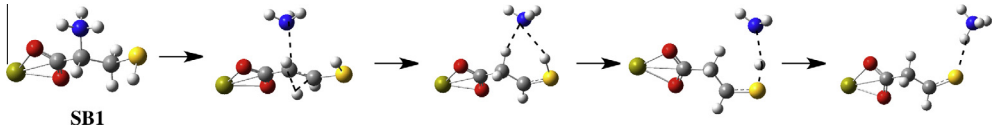

Scheme 1. Structural changes along the **CE1** Coulomb explosion.

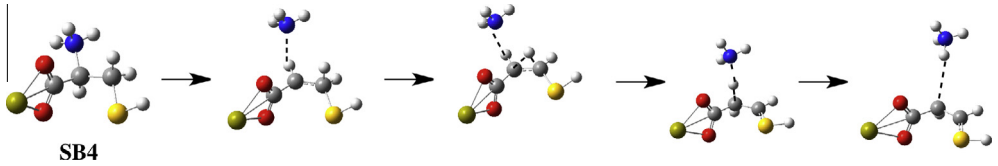

Scheme 2. Structural changes along the **CE2** Coulomb explosion.

It is also worth noting that whereas for reaction **AL1** the minimum of the chemical potential coincides with position of the activation barrier, i.e., for the TS structure, for **AL2**, where the top of the barrier is closer to the products, the minimum of the chemical potential appears slightly shifted toward the reactants. For both cases, the profile of the REF is the one expected, with maximum and minimum values in the interphase reactant-TS and TS-products, whereas it becomes zero at the top of the activation barrier for the **AL1** reaction, whereas for the **AL2** process this happens for values of the reaction coordinate closer to the reactants. There are however, some subtle differences between both processes, which become more evident when looking at the corresponding REFs. For **AL1** there is a small oscillation of the REF in the reactants region, which is not observed for **AL2**, whereas for the latter there is a shoulder within the TS region (between ξ_2 and ξ_3) which is not observed in the former. Indeed, in the **AL1** process an internal rotation of the NH_3 moiety breaks the S···H–NH_2 hydrogen bond of the reactant, before the cleavage of the C–NH_3 bond takes place. The cleavage of the aforementioned intramolecular hydrogen bond is responsible for the small maximum observed in the **AL1** REF. The shoulder observed in reaction **AL2** in the TS region is due to the formation of a hydrogen bond between the NH_3 leaving molecule,

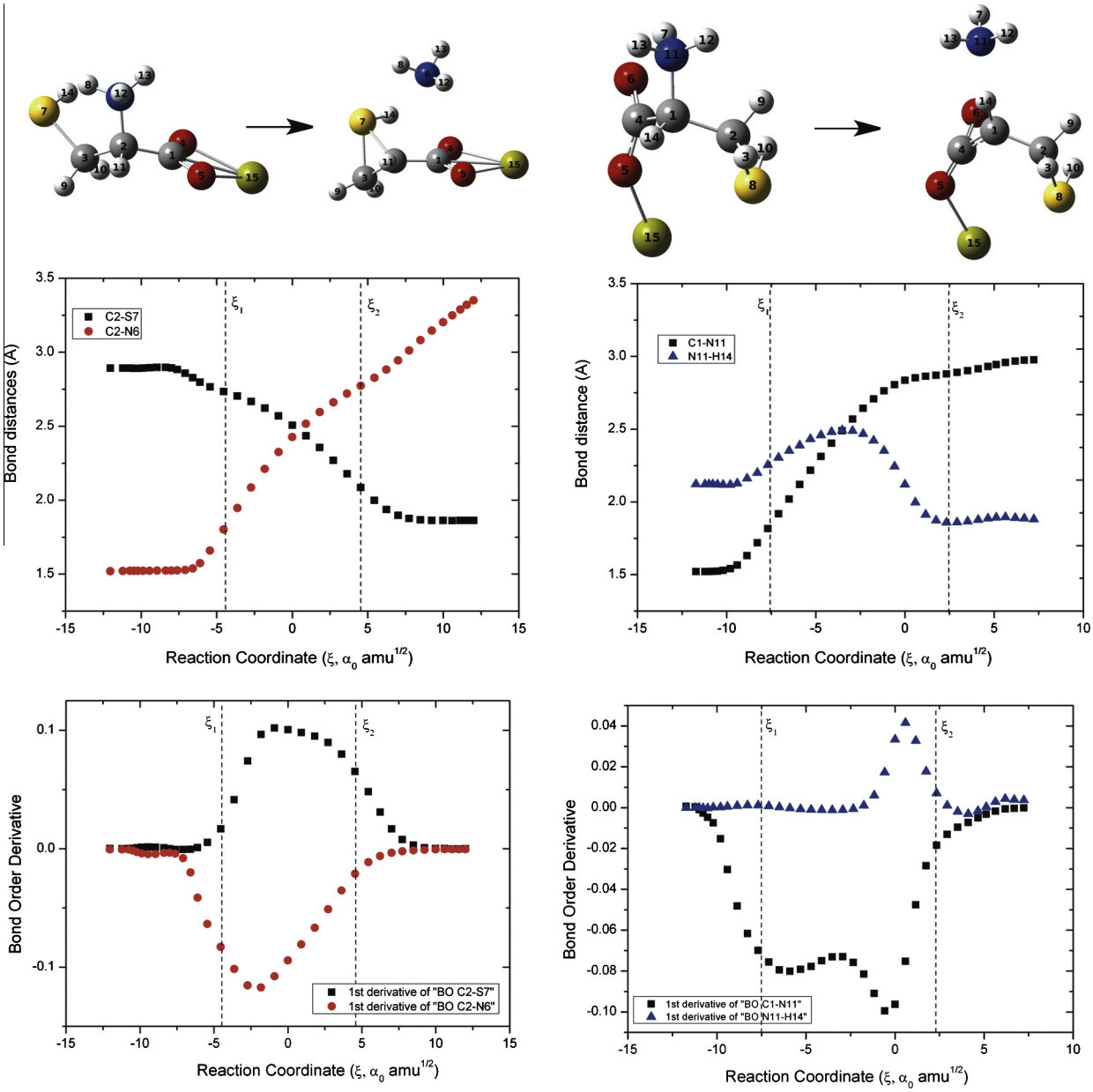

Fig. 6. Evolution of some relevant bond distances (Å) and bond order derivatives (a.u.) for **AL1** and **AL2** processes along the reaction coordinate.

acting as proton acceptor, and the CH group, bonded to the carboxylate group, acting as proton donor.

The evolution of the chemical potential and the REF for both Coulomb explosions is more complex than for the ammonia-loss processes. Analyzing first the **CE2** reaction, it is apparent that the behavior of the chemical potential within the ξ_1 and ξ_2 limits is rather similar to the one found for both ammonia-loss processes, with a minimum at the center of the region and two similar maxima at the boundaries, indicating that the fragmentation of the C–NH_3 is the dominant mechanism within this region. The behavior of the REF is also similar to that found for the **AL1** and **AL2** reactions, showing a maximum and a minimum at the ξ_1 and ξ_2 points, respectively. After ξ_2 the chemical potential decreases again to increase abruptly at ξ_3. This second minimum within the ξ_2–ξ_3 region is associated with the formation of the new N–H bond to yield NH_4^+. As expected the REF shows now a maximum and a minimum at ξ_2 and ξ_3 points respectively.

The profiles for **CE1** seem very different from those of **CE2**, but again the chemical potential inside the ξ_1 and ξ_2 limits is essentially equal, with the only difference that the ξ_2 limit appears earlier than in the **CE2** reaction and therefore the value of the chemical potential at this point is much smaller than at ξ_1, whereas for **CE2** both values were almost equal. After ξ_2 the chemical potential also decreases for **CE1**, but differently to the **CE2** process, two minima appear within the ξ_2–ξ_3 region. This seems to indicate that not only one but two processes take place within this region. Indeed, a close examination of the whole energy profile (see Scheme 1) shows that almost simultaneously with the C–NH_3 bond cleavage, a proton transfer from the CH_2 group attached to SH toward the C atom from which the NH_3 fragment is leaving, occurs. The partial overlap between the C–NH_3 bond cleavage and this proton transfer also explains why the ξ_2 boundary appears earlier. The subsequent step would be a second proton transfer from the SH group toward the ammonia molecule to form the ammonium

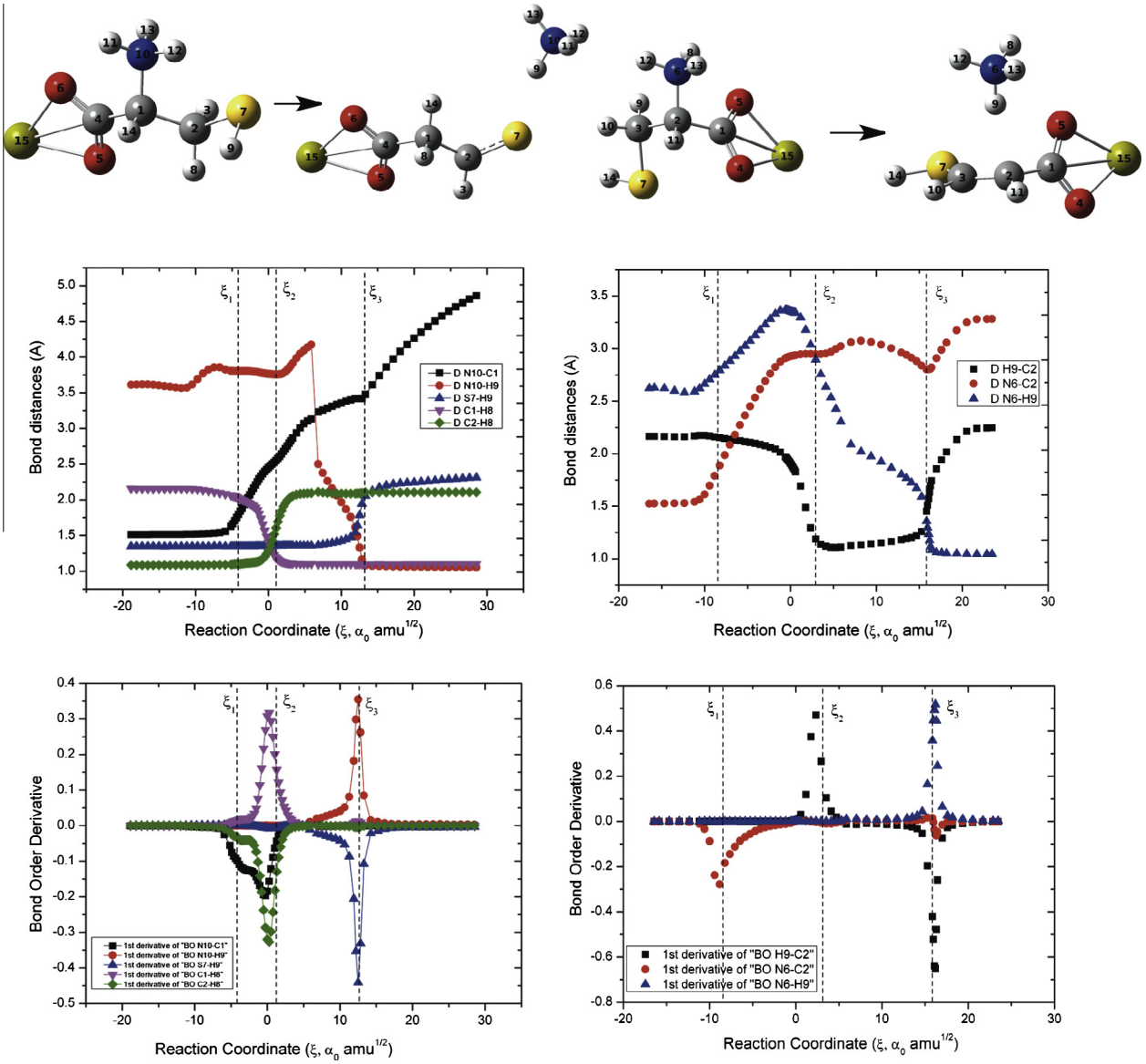

Fig. 7. Evolution of some relevant bond distances (Å) and bond order derivatives (a.u.) for **CE1** and **CE2** processes along the reaction coordinate.

ion, and which would be responsible of the appearance of the second minimum in the chemical potential.

Coherently, the REF exhibits besides the maximum and the minimum at ξ_2 and ξ_3 as observed in the **CE2** reaction, one additional maximum and one additional minimum within the ξ_2–ξ_3 region, associated to the aforementioned extra proton transfer. In summary, in the **CE1** Coulomb explosion three elementary process concur, the C–NH_3 bond cleavage which occurs almost simultaneously with a first $CH_2 \rightarrow CH$ proton transfer, followed by a second proton transfer from the SH group toward the ammonia molecule. The **CE2** Coulomb explosion also initiates with the C–NH_3 bond cleavage, followed by the formation of a C–H···NH_3 hydrogen bond. The final transfer of this C–H proton toward the ammonia molecule is assisted by the arrival of a second proton coming from the CH_2 group attached to SH, in a kind of assisted proton transfer mechanism [40] (see Scheme 2).

3.3. Evolution of bond distances and variation of bond orders

The evolution of the relevant bond distances and, in particular of the variation of the corresponding bond orders, offers a nice complement to improve the picture of the fine details of the mechanisms involved in these reactions. These variations for the **AL1** and **AL2** processes are given in Fig. 6.

For **AL1** the breaking of the C2–N6 bond and the formation of the C2–S7 bond are the main changes in the TS region. However, the C2–N6 breaking initiates in the reactant zone and the C2–S7 forming, with the appearance of its BCP, in the product region, indicating that electronic changes are not only restricted to the TS zone. However, as indicated by the derivatives of the bond orders, the maximum variation takes place in both cases within the TS state region and close to the limit ξ_1 with the reactants region (see Fig. 7).

For **AL2**, the breaking of C1–N11 bond also starts in the reactant zone and it is almost complete before entering in the product region, where this distance remains almost constant. This seems to be consistent with the maximum variation of the C1–N11 bond order occurring within the TS region but close to the limit ξ_2 with the products region, and is the consequence of the formation of the hydrogen bond between ammonia as proton acceptor and one of the CH_2 groups as proton donor. The formation of this hydrogen bond starts in the TS region as reflected by a sizable decrease of

the N11–H14 internuclear distance, and the maximum observed for the variation of the corresponding bond order.

For reactions **CE1** and **CE2** the number of relevant bond distances that change along the reaction coordinate is larger. For **CE1**, in slight contrast with the ammonia-loss reactions, no significant changes in the distances are observed in the reactants region as most of them begin within the TS region. It can be observed, in agreement with our previous discussion that the C–NH_3 (C1–N10) bond cleavage (black curve) occurs almost simultaneously with the proton transfer from C2H8 toward C1, so the C2–H8 distance increases (green curve) whereas the C1–H8 distance decreases (purple curve). It is worth noting by looking at the position of the maxima for the variation of the corresponding bond orders, that this process is almost complete when the ξ_2 point is reached. However, after this point the C1–N10 distances continues to increase further until reaching the ξ_3 point, in which position the distance between the ammonia molecule and the H atom of the SH group is small enough to favor the proton transfer from the latter toward the former. Hence, the S–H distance starts increasing near that region and concomitantly the N10–H9 decreases dramatically from ξ_2 to ξ_3. After ξ_3 both distances remain practically constant because the NH_4^+ is already formed. Consistently, the maxima and minima of the corresponding bond orders appear at ξ_3.

The situation is simpler for **CE2** process, because as discussed above, only two elementary reactions are involved. The most significant changes affect the C2–N6 distance involved in the C–NH_3 bond cleavage and the N6–H9, which corresponds to the proton transfer from the methylene group attached to SH toward the ammonia molecule. The C2–N6 distance begins to increase already in the reactants region and becomes practically constant when the ξ_2 point is reached. Within the ξ_2–ξ_3 region shows small variations to increase further after ξ_3 when entering in the products region. Note that, coherently, the most significant bonding change occurs very early, in the boundary between the reactants and the TS regions where the variation of the bond order presents a minimum. The next significant change in the variation of the C2–N6 bond order takes place at ξ_3, because around this area the NH_3 molecule reorients itself to favor the formation of a $H_3NH^+\cdots C$ ionic hydrogen bond (see Fig. 3) what approaches the H to the C2 carbon but move away the N atom. The most significant change in the N6–H9 distance takes place inside the ξ_2–ξ_3 region, but the most dramatic change in the variations of the bond order occurs precisely at ξ_3 where the derivative of the corresponding bond order presents a sharp maximum.

4. Conclusions

A detailed analysis of the loss of ammonia and the formation of ammonium ion, which are the dominant peaks in the MS/MS spectrum of $[Ca(Cys)]^{2+}$ in the gas phase, in terms of the profiles of the reaction force, the chemical potential and the REF permits to obtain interesting insights into the details of the mechanisms involved in both kind of processes. These analyses show that all the ammonia-loss processes can be considered essentially as elementary reactions, whereas the two Coulomb explosions investigated involve more than one elementary step. Our survey shows that for the **CE2** reaction two elementary steps are involved, and three for the **CE1** one. The description in terms of the variations of the chemical potential and in particular of the REF permits to identify very easily the subtle differences that exist between two processes, such as **AL1** and **AL2** which apparently are essentially equal. The same applies to **CE1** and **CE2** reactions. The bond breaking and the bond formation processes can be followed through the evolution of the corresponding internuclear distances along the reaction coordinate; but the most precise information on where the bond formation or the bond fissions are complete is readily obtained by plotting the derivatives of the corresponding bond orders along the reaction coordinate.

Acknowledgements

This work has been partially supported by the Ministerio de Economía y Competitividad of Spain (Project No. CTQ2012-35513-C02-01), by the CMST COST Action CM1204, and by the Project MADRISOLAR2, Ref.: S2009PPQ/1533 of the Comunidad Autónoma de Madrid and by FONDECYT 1120093 y el ICM N° 120082 of Chile. Computational time at Centro de Computación Científica (CCC) of Universidad Autónoma de Madrid is also acknowledged. MH wishes to dedicate this paper to the memory of Prof. Julio Guillermo Contreras Koder.

References

[1] M. Alcamí, O. Mó, M. Yáñez, Computational chemistry. A useful (sometimes mandatory) tool in mass spectrometry studies, Mass Spectrom. Rev. 20 (2001) 195–245.
[2] W. Koch, H. Schwarz, F. Maquin, D. Stahl, On the formation of doubly charged cation radicals from acetyl and 1-hydroxyvinyl cations in the gas-phase – a combined experimental and ab initio study, Int. J. Mass Spectrom. 67 (1985) 171–177.
[3] H. Nair, A. Somogyi, V.H. Wysocki, Effect of alkyl substitution at the amide nitrogen on amide bond cleavage: electrospray ionization surface-induced dissociation fragmentation of substance P and two alkylated analogs, J. Mass Spectrom. 31 (1996) 1141–1148.
[4] E.E. Rennie, C.A.F. Johnson, J.E. Parker, R. Ferguson, D.M.P. Holland, D.A. Shaw, A photoabsorption and mass spectrometry study of pyrrole, Chem. Phys. 250 (1999) 217–236.
[5] J.L. Seymour, F. Turecek, Structure, energetics and reactivity of ternary complexes of amino acids with Cu(II) and 2,2′-bipyridine by density functional theory. A combination of radical-induced and spin-remote fragmentations, J. Mass Spectrom. 37 (2002) U533–U534.
[6] J.Y. Salpin, J. Tortajada, Gas-phase reactivity of lead(II) ions with D-glucose. Combined electrospray ionization mass spectrometry and theoretical study, J. Phys. Chem. A 107 (2003) 2943–2953.
[7] I. Corral, O. Mó, M. Yáñez, J.-Y. Salpin, J. Tortajada, L. Radom, Gas-phase reactions between urea and Ca^{2+}: the importance of Coulomb explosions, J. Phys. Chem. A 108 (2004) 10080–10088.
[8] E. Constantino, L. Rodríguez-Santiago, M. Sodupe, J. Tortajada, Interaction of Co^+ and Co^{2+} with glycine. A theoretical study, J. Phys. Chem. A 109 (2005) 224–230.
[9] H.J. Zhai, X. Huang, T. Waters, X.B. Wang, R.A.J. O'Hair, A.G. Wedd, L.S. Wang, Photoelectron spectroscopy of doubly and singly charged group VIB dimetalate anions: $M_2O_7^{2-}$, MM′O-7(2-), and $M_2O_7^-$ (M, M′ = Cr, Mo, W), J. Phys. Chem. A 109 (2005) 10512–10520.
[10] I. Corral, O. Mó, M. Yáñez, J.Y. Salpin, J. Tortajada, D. Moran, L. Radom, An experimental and theoretical investigation of gas-phase reactions of Ca^{2+} with glycine, Chem. Eur. J. 12 (2006) 6787–6796.
[11] J.W. Jones, T. Sasaki, D.R. Goodlett, F. Turecek, Electron capture in spin-trap capped peptides. An experimental example of ergodic dissociation in peptide cation-radicals, J. Am. Soc. Mass Spectrom. 18 (2007) 432–444.
[12] A.M. Lamsabhi, M. Alcamí, O. Mó, M. Yáñez, J. Tortajada, J.Y. Salpin, Unimolecular reactivity of uracil-$Cu^{2(+)}$ complexes in the gas phase, ChemPhysChem 8 (2007) 181–187.
[13] J. Chamot-Rooke, C. Malosse, G. Frison, F. Turecek, Electron capture in charge-tagged peptides. Evidence for the role of excited electronic states, J. Am. Soc. Mass Spectrom. 18 (2007) 2146–2161.
[14] M. Girod, Y. Carissan, S. Humbel, L. Charles, Tandem mass spectrometry of doubly charged poly(ethylene oxide) oligomers produced by electrospray ionization, Int. J. Mass Spectrom. 272 (2008) 1–11.
[15] J. Fiser, K. Franzreb, J. Lorincik, P. Williams, Oxygen-containing diatomic dications in the gas phase, Eur. J. Mass Spectrom. 15 (2009) 315–324.
[16] J.-Y. Salpin, S. Guillaumont, J. Tortajada, A.M. Lamsabhi, Gas-phase interactions between lead(II) ions and thiouracil nucleobases: a combined experimental and theoretical study, J. Am. Soc. Mass Spectrom. 20 (2009) 359–369.
[17] A. Eizaguirre, A.M. Lamsabhi, O. Mó, M. Yáñez, Assisted intramolecular proton transfer in (uracil)(2)Ca^{2+} complexes, Theor. Chem. Acc. 128 (2011) 457–464.
[18] V. Brites, K. Franzreb, M. Hochlaf, Metastable ClO^{2+} and ClO^{3+} ions in the gas phase: a combined theoretical and mass spectrometric investigation, Phys. Chem. Chem. Phys. 13 (2011) 18315–18321.
[19] E.J.H. Yoo, L. Feketeova, G.N. Khairallah, R.A.J. O'Hair, Unimolecular chemistry of doubly protonated zwitterionic clusters, J. Phys. Chem. A 115 (2011) 4179–4185.
[20] C. Trujillo, A.M. Lamsabhi, O. Mó, M. Yáñez, J.-Y. Salpin, Unimolecular reactivity upon collision of uracil-Ca^{2+} complexes in the gas phase: comparison with uracil-M^+ (M = H, alkali metals) and uracil-M^{2+} (M = Cu, Pb) systems, Int. J. Mass Spectrom. 306 (2011) 27–36.

[21] S.Q. Zhang, L. Xu, J.G. Dong, P. Cheng, Z. Zhou, J.M. Fu, Collision-induced dissociation of singly and doubly charged Cu-II-cytidine complexes in the gas phase: an experimental and computational study, RSC Adv. 2 (2012) 2568–2575.
[22] S. Maclot, D.G. Piekarski, A. Domaracka, A. Mery, V. Vizcaino, L. Adoui, F. Martín, M. Alcamí, B.A. Huber, P. Rousseau, S. Díaz-Tendero, Dynamics of glycine dications in the gas phase: ultrafast intramolecular hydrogen migration versus Coulomb repulsion, J. Phys. Chem. Lett. 4 (2013) 3903–3909.
[23] M. Hurtado, M. Monte, A.M. Lamsabhi, M. Yáñez, O. Mó, J.-Y. Salpin, Modeling interactions between an amino acid and a metal dication: cysteine–calcium(II) reactions in the gas phase, ChemPlusChem 78 (2013) 1124–1133.
[24] J. Martínez, A. Toro-Labbé, The reaction force. A scalar property to characterize reaction mechanisms, J. Math. Chem. 45 (2009) 911–927.
[25] A. Toro-Labbé, Characterization of chemical reactions from the profiles of energy, chemical potential, and hardness, J. Phys. Chem. A 103 (1999) 4398–4403.
[26] A.M. Lamsabhi, O. Mó, S. Gutiérrez Oliva, P. Pérez, A. Toro Labbé, M. Yáñez, The mechanism of double proton transfer in dimers of uracil and 2-thiouracil—the reaction force perspective, J. Comput. Chem. 30 (2009) 389–398.
[27] P. Politzer, A. Toro-Labbé, S. Gutiérrez-Oliva, B. Herrera, P. Jaque, M.C. Concha, J.S. Murray, The reaction force: three key points along an intrinsic reaction coordinate, J. Chem. Sci. 117 (2005) 467–472.
[28] P. Politzer, A. Toro-Labbé, S. Gutiérrez-Oliva, J.S. Murray, Perspectives on the reaction force, in: J.R. Sabin, E.J. Brandas (Eds.), Advances in Quantum Chemistry, vol. 64, Elsevier B.V., 2012, pp. 189–209.
[29] A. Toro-Labbé, S. Gutiérrez-Oliva, J. Murray, P. Politzer, The reaction force and the transition region of a reaction, J. Mol. Mod. 15 (2009) 707–710.
[30] P. Flores-Morales, S. Gutiérrez-Oliva, E. Silva, A. Toro-Labbé, The reaction electronic flux: a new descriptor of the electronic activity taking place during a chemical reaction. Application to the characterization of the mechanism of the Schiff's base formation in the Maillard reaction, J. Mol. Struct. THEOCHEM 943 (2010) 121–126.
[31] P. Politzer, J.S. Murray, P. Lane, A. Toro-Labbé, A noteworthy feature of bond dissociation/formation reactions, Int. J. Quant. Chem. 107 (2007) 2153–2157.
[32] M.L. Ceron, E. Echegaray, S. Gutiérrez-Oliva, B. Herrera, A. Toro-Labbé, The reaction electronic flux in chemical reactions, Sci. China-Chem. 54 (2011) 1982–1988.
[33] A.D. Becke, Density-functional thermochemistry. III. The role of exact exchange, J. Chem. Phys. 98 (1993) 5648.
[34] C. Lee, W. Yang, R.G. Parr, Development of the Colle–Salvetti correlation-energy formula into a functional of the electron density, Phys. Rev. B 37 (1988) 785.
[35] C. Gonzalez, H.B. Schlegel, Reaction-path following in mass-weighted internal coordinates, J. Phys. Chem. 94 (1990) 5523–5527.
[36] M.J.T. Frisch, G.W. Schlegel, H.B. Scuseria, G.E. Robb, M.A. Cheeseman, J.R. Scalmani, G. Barone, V. Mennucci, B. Petersson, G.A. Nakatsuji, H. Caricato, M. Li, X. Hratchian, H.P. Izmaylov, A.F. Bloino, J. Zheng, G. Sonnenberg, J.L. Hada, M. Ehara, M. Toyota, K. Fukuda, R. Hasegawa, J. Ishida, M. Nakajima, T. Honda, Y. Kitao, O. Nakai, H. Vreven, T. Montgomery Jr., J.A. Peralta, J.E. Ogliaro, F. Bearpark, M. Heyd, J.J. Brothers, E. Kudin, K.N. Staroverov, V.N. Kobayashi, R. Normand, J. Raghavachari, K. Rendell, A. Burant, J.C. Iyengar, S.S. Tomasi, J. Cossi, M. Rega, N. Millam, J.M. Klene, M. Knox, J.E. Cross, J.B. Bakken, V. Adamo, C. Jaramillo, J. Gomperts, R. Stratmann, R.E. Yazyev, O. Austin, A.J. Cammi, R. Pomelli, C. Ochterski, J.W. Martin, R.L. Morokuma, K. Zakrzewski, V.G. Voth, G.A. Salvador, P. Dannenberg, J.J. Dapprich, S. Daniels, A.D. Farkas, Ö. Foresman, J.B. Ortiz, J.V. Cioslowski, D.J. Fox, Gaussian09, Gaussian Inc., Wallingford, CT, 2010.
[37] F. Weinhold, C.R. Landis, Valency and Bonding, Cambridge University Press, Cambridge, 2005.
[38] C.F. Matta, R.J. Boyd, The Quantum Theory of Atoms in Molecules, Wiley-VCH Verlag GmbH & Co., KGaA, Weinheim, 2007.
[39] R.F.W. Bader, Atoms in Molecules: A Quantum Theory, Clarendon Press Oxford Univ., Oxford, 1990.
[40] A. Eizaguirre, A.M. Lamsabhi, O. Mó, M. Yáñez, Assisted intramolecular proton transfer in (uracil)2Ca^{2+} complexes, Theoret. Chem. Acc. 128 (2011) 457–464.